
From Rank Estimation to Rank Approximation: Rank Residual Constraint for Image Denoising

Zhiyuan Zha¹, Xin Yuan², Tao Yue¹, Jiaotao Zhou³

¹Department of Electronic Science and Engineering, Nanjing University, Nanjing 210023, China.

²Nokia Bell Labs, 600 Mountain Avenue, Murray Hill, NJ, 07974, USA.

³Department of Computer and Information Science, University of Macau, Macau 999078, China.

zhazhiyuan.mmd@gmail.com, xyuan@bell-labs.com, yuetao@nju.edu.cn, jtzhou@umac.mo.

Abstract

Inspired by the recent advances of Generative Adversarial Networks (GAN) in deep learning, we propose a novel rank minimization approach, termed rank residual constraint (RRC), for image denoising in the optimization framework. Different from GAN, where a discriminative model is trained jointly with a generative model, in image denoising, since the labels are not available, we build an unsupervised mechanism, where two generative models are employed and jointly optimized. Specifically, by integrating the image nonlocal self-similarity prior with the proposed RRC model, we develop an iterative algorithm for image denoising. We first present a recursive based nonlocal means approach to obtain a good reference of the original image patch groups, and then the rank residual of image patch groups between this reference and the noisy image is minimized to achieve a better estimate of the desired image. In this manner, both the reference and the estimated image in each iteration are improved gradually and jointly; in the meantime, we progressively *approximate* the underlying low-rank matrix (constructed by image patch groups) via minimizing the rank residual, which is different from existing low-rank based approaches that estimate the underlying low-rank matrix directly from the corrupted observation. We further provide a theoretical analysis on the feasibility of the proposed RRC model from the perspective of group-based sparse representation. Experimental results demonstrate that the proposed RRC model outperforms many state-of-the-art denoising methods.

1 Introduction

The Generative Adversarial Networks (GAN) [43] have led to significant improvements on various tasks in deep learning [47, 44–46]. While one research direction is to apply the GAN to other applications, in this paper, we consider to utilize the underlying principle of GAN in the traditional optimization framework, more specifically, in the unsupervised image restoration task. Recall that in GAN, a discriminative model is trained jointly with a generative model, and the competition between these two models will drive the generated samples to be indistinguishable from real data. Motivated by this significant success, we aim to answer the following questions in this paper.

- i) Can we use the principle or the similar spirit of GAN in the traditional (unsupervised) optimization framework?
- ii) How to build such a (jointly competitive) model in the optimization regime?
- iii) Is there an efficient and theoretical analyzable algorithm to solve such a competitive model?

We address these questions by proposing a new rank minimization model, dubbed rank residual constraint (RRC) for image denoising. In a nutshell, given the corrupted (vectorized) image y , by

integrating the image nonlocal self-similarity (NSS) prior [24–26] with the proposed RRC model, in each iteration, we construct a reference low-rank matrix X' (for each image patch group) by developing a recursive based nonlocal means approach, and drive our recovered matrix \hat{X} to this reference via the proposed RRC minimization algorithm. Note that the reference matrix X' and the recovered matrix \hat{X} serve as the two competitive generative models in our proposed unsupervised mechanism; both of them are improved gradually and jointly in each iteration, and via minimizing the rank residual between them, better results can be achieved. The flowchart of the proposed RRC model for image denoising is illustrated in Fig. 1.

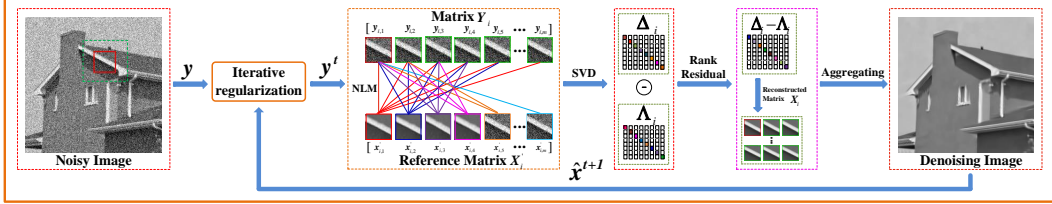


Figure 1: Flowchart of the proposed RRC model for image denoising. The reference matrix X' and estimated matrix \hat{X} are jointly optimized and driven by the *rank residual* to be close to each other in each iteration.

We develop an efficient algorithm to solve the proposed RRC model by imposing a Laplacian prior on the rank residual between X' and \hat{X} . Fig. 2 demonstrates that the reconstructed image from our proposed algorithm can progressively approximate the ground truth, by taking the *House* image as an example, which is corrupted by zero-mean Gaussian noise with standard deviation $\sigma_n=100$. It can be observed that the singular values of the reference matrix X' approaches the singular values of the ground truth progressively (Fig. 2 (b-d)) and so does the recovered image (Fig. 2 (f-h)). Moreover, we provide a theoretical analysis on the feasibility of the proposed RRC model from the perspective of the group-based sparse representation, which is detailed in Section 5.

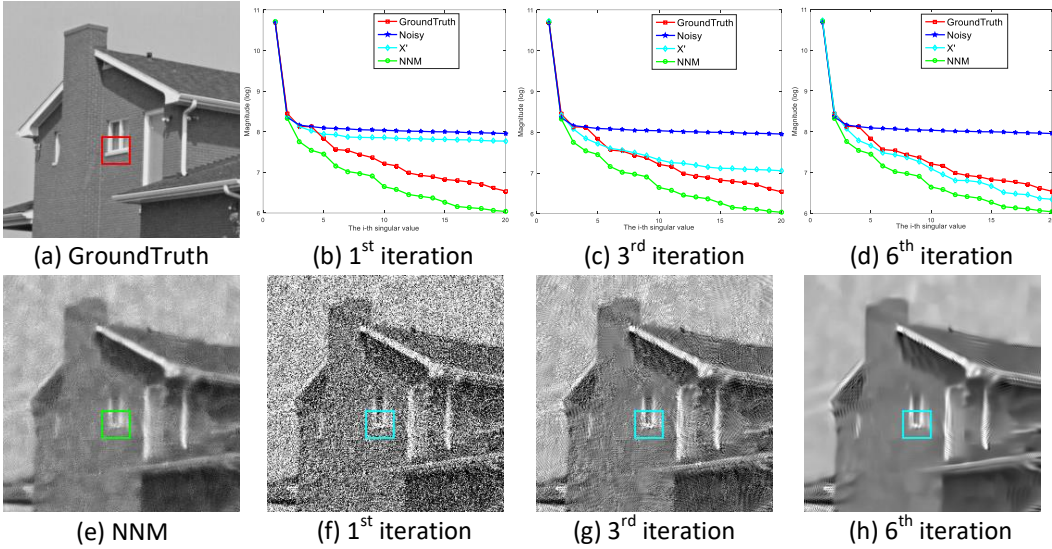


Figure 2: Illustration of the proposed image denoising method via rank residual constraint (RRC). The *House* image is corrupted by Gaussian noise with $\sigma_n=100$. (b-d) The singular values of the image patch group (with reference in the red box in (a)) from ground truth image (red), noisy image (blue), image recovered by the well-known nuclear norm minimization method (NNM, green) [15] and the proposed reference matrix X' (cyan) at the 1st, 3rd and 6th iterations of our algorithm. (f-h) Reconstructed images at the 1st, 3rd and 6th iterations using the proposed RRC model. It can be observed that the singular values of X' progressively approach the ground truth and the reconstructed image is getting close to the original image.

The rest of this paper is organized as follows. Section 2 introduces the previous low rank matrix estimation works. Section 3 develops the RRC model based on the rank minimization scenario. Section 4 drives the algorithm to solve the RRC model for image denoising by integrating the image NSS prior. Section 5 derives a theoretical analysis of the proposed RRC model in terms of

group-based sparse representation. Section 6 presents the experimental results for image denoising and Section 7 concludes the paper.

2 Related Work

Low-rank matrix estimation aims to recover the underlying low-rank matrix from its degraded observation, which has a variety of applications in computer vision and machine learning [1, 9, 6, 5, 4, 3, 2, 10, 8]. In image processing, since the matrix constructed by *nonlocal* similar patches in a natural image is of low rank, a flurry of low-rank matrix estimation methods have been proposed for various tasks, such as image alignment [2], video denoising [4], shadow removal [1] and reconstruction of occluded/corrupted face images [3]. One typical low-rank matrix estimation method is the low-rank matrix factorization [6, 3, 13, 12, 11], which factorizes the observed matrix \mathbf{Y} into the product of two matrices that can be used to reconstruct the desired matrix with certain fidelity. A parallel research is the rank minimization methods [15, 9, 5, 16, 7, 21, 19, 22, 20, 18, 17], with the nuclear norm minimization (NNM) [15, 5] being the most representative approach. The nuclear norm of a matrix \mathbf{X} , denoted by $\|\mathbf{X}\|_*$, is the summation of its singular values, i.e., $\|\mathbf{X}\|_* = \sum_i \sigma_i$, with σ_i representing the i^{th} singular value of \mathbf{X} . NNM aims to recover the underlying low rank matrix \mathbf{X} from its degraded observation matrix \mathbf{Y} , while minimizing $\|\mathbf{X}\|_*$. However, NNM usually tends to over-shrink the rank components (Fig. 2, green curves in (b-d)), and thus limits its capability and flexibility. To improve the flexibility of NNM, most recently, Gu *et al.* [7] proposed the weighted nuclear norm minimization (WNNM) model, which is essentially the reweighted ℓ_1 -norm [23] of the singular values of the desired matrix. Compared with NNM, WNNM assigns different weights to different singular values such that the matrix rank estimation becomes more accurate. Similar case also exists in the truncated nuclear norm minimization [21] and weighted Schatten p -norm [17] minimization problems.

However, one common property of the aforementioned low-rank models is to *estimate* the low-rank matrix only from the corrupted observation and this may lead to inaccurate results in real applications such as the image inverse problems. Bearing this in mind, in this paper, we analyze the rank minimization problem from the perspective of matrix *approximation* by proposing the RRC model. By integrating the image NSS prior with the proposed RRC model, we develop an iterative algorithm for image denoising. To this end, a recursive based nonlocal means approach is first employed to obtain a good reference of the original image patch groups, and then the rank residual of image patch groups between this reference and the noisy image is minimized to achieve a better estimate of the desired image. The reference and the estimated image are alternately updated in each iteration and thus compete with each other (as in GAN) while both being improved gradually and jointly.

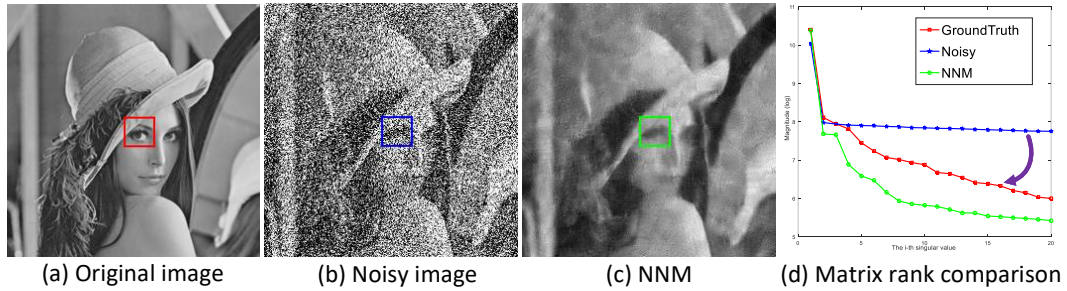


Figure 3: Analyzing the matrix rank by image denoising.

3 Rank Minimization via Rank Residual Constraint

3.1 Nuclear Norm Minimization

According to [5], nuclear norm is the tightest convex relaxation of the original rank minimization problem. Given a data matrix $\mathbf{Y} \in \mathbb{R}^{d \times m}$, the goal of NNM is to find a matrix $\mathbf{X} \in \mathbb{R}^{d \times m}$ of rank $r \leq \min(d, m)$, by solving

$$\hat{\mathbf{X}} = \arg \min_{\mathbf{X}} \left(\frac{1}{2} \|\mathbf{Y} - \mathbf{X}\|_F^2 + \lambda \|\mathbf{X}\|_* \right), \quad (1)$$

where $\|\cdot\|_F^2$ denotes the Frobenius norm and $\lambda > 0$ is the regularization parameter. Candès *et al.* [9] proved that the low-rank matrix can be perfectly recovered from the degraded/corrupted data

matrix with high probability by solving an NNM problem. Despite the theoretical guarantee of the singular value thresholding (SVT) algorithm [15], it has been observed that the recovery performance of such a convex relaxation will degrade in the presence of noise, and the solution can seriously deviate from the original solution of rank minimization problem [17]. More specifically, NNM tends to over-shrink the rank of the matrix. Taking the image *Lena* in Fig. 3(a) as an example, we add Gaussian noise with standard deviation $\sigma_n=100$ to the clean image and perform NNM to recover a denoised image in Fig. 3(c). We randomly extract a patch from the noisy image in Fig. 3(b) and search 60 similar patches to generate a group. These patches (after vectorization) in this group are then stacked into a data matrix (please refer to Section 4 for details of constructing the group). Since all the patches in this group have similar structures, the constructed data matrix is of low rank. Based on this, we plot the singular values of the patch group in the noisy image, NNM recovered image and the original image in Fig. 3(d). As can be seen, the solution of NNM (green line) is severely deviated (over-shrink) from the ground truth (red line).

3.2 Rank Residual Constraint

As demonstrated in Fig. 3, due to the influence of noise, it is difficult to estimate the matrix rank precisely using NNM. More specifically, in Fig. 3(d), the singular values of the observed matrix are seriously deviated from the singular values of the original matrix. However, in low-rank matrix estimation, we wish that the singular values of the recovered matrix \mathbf{X} and the singular values of the original matrix \mathbf{X}^* are as close as possible. Explicitly, we define the *rank residual* by

$$\boldsymbol{\gamma}^* = \boldsymbol{\sigma} - \boldsymbol{\psi}^*, \quad (2)$$

where $\boldsymbol{\sigma}$ and $\boldsymbol{\psi}^*$ are the singular values of \mathbf{X} and \mathbf{X}^* , respectively. It can be seen that the rank estimation of the matrix \mathbf{X} largely depends on the level of this rank residual.

However, in real applications, the original matrix \mathbf{X}^* is not available, and thus we desire a good *estimate* of it, denoted by \mathbf{X}' . Via introducing this \mathbf{X}' and defining $\boldsymbol{\gamma} = \boldsymbol{\sigma} - \boldsymbol{\psi}$ with $\boldsymbol{\psi}$ being the singular values of \mathbf{X}' , we propose the *rank residual constraint* (RRC) model below,

$$\hat{\mathbf{X}} = \arg \min_{\mathbf{X}} \left(\frac{1}{2} \|\mathbf{Y} - \mathbf{X}\|_F^2 + \lambda \|\boldsymbol{\gamma}\|_{S_p} \right), \quad (3)$$

where S_p denotes some type of norm for regularization analyzed in subsection 4.1. We will describe how to estimate \mathbf{X}' and solve Eq. (3) below. Specifically, we apply the proposed RRC model to image denoising in the following section.

4 Image Denoising via Rank Residual Constraint

Image denoising [24, 25, 29, 26, 28, 27] is not only an important problem in image processing, but also an ideal test bench to measure different statistical image models. Mathematically, image denoising aims to recover the latent clean image \mathbf{x} from its noisy observation $\mathbf{y} = \mathbf{x} + \boldsymbol{\eta}$, where $\boldsymbol{\eta}$ is usually assumed to be zero-mean Gaussian noise with standard deviation σ_n . Owing to the ill-posed nature of image denoising, it is critical to exploit the prior knowledge that characterizes the statistical features of the image. The well-known NSS prior [24, 25, 29, 26, 28, 30], which investigates the repetitiveness of textures and structures of natural images within nonlocal regions, implies that many similar patches can be found given a reference patch.

To be concrete, a noisy (vectorized) image $\mathbf{y} \in \mathbb{R}^N$ is divided into n overlapping patches of size $\sqrt{d} \times \sqrt{d}$, and each patch is denoted by a vector $\mathbf{y}_i \in \mathbb{R}^d, i = 1, 2, \dots, n$. For the i^{th} patch \mathbf{y}_i , its m similar patches are selected from a surrounding (searching) window with $L \times L$ pixels to form a set \mathcal{S}_i . After this, these patches in \mathcal{S}_i are stacked into a matrix $\mathbf{Y}_i \in \mathbb{R}^{d \times m}$, i.e., $\mathbf{Y}_i = \{\mathbf{y}_{i,1}, \mathbf{y}_{i,2}, \dots, \mathbf{y}_{i,m}\}$. This matrix \mathbf{Y}_i consisting of patches with similar structures is thus called a group, where $\{\mathbf{y}_{i,j}\}_{j=1}^m$ denotes the j^{th} patch in the i^{th} group. Then we have $\mathbf{Y}_i = \mathbf{X}_i + \mathbf{N}_i$, where \mathbf{X}_i and \mathbf{N}_i are the corresponding group matrices of the original image and noise, respectively. Since all patches in each data matrix have similar structures, the constructed data matrix \mathbf{Y}_i is of low rank. By adopting the proposed RRC model in Eq. (3), the low rank matrix \mathbf{X}_i can be estimated by solving

$$\hat{\mathbf{X}}_i = \arg \min_{\mathbf{X}_i} \left(\frac{1}{2} \|\mathbf{Y}_i - \mathbf{X}_i\|_F^2 + \lambda \|\boldsymbol{\gamma}_i\|_{S_p} \right), \quad (4)$$

where $\gamma_i = \sigma_i - \psi_i$, with σ_i and ψ_i representing the singular values of X_i and X'_i , respectively; $X'_i \in \mathbb{R}^{d \times m}$ is a good estimate of the original image patch group X_i^* . In order to achieve a high performance for image denoising, we hope that the rank residual γ_i of each group is small enough.

4.1 Determine S_p

Let us come back to Eq. (4). Obviously, one important issue of our RRC based image denoising is the determination of S_p . Hereby, we perform some experiments to investigate the statistical property of γ , where γ denotes the set of $\gamma_i = \sigma_i - \psi_i$ and we use the original image x to construct X' . In these experiments, two typical images *Fence* and *Parrot* are corrupted by Gaussian noise with standard deviations $\sigma_n=20$ and $\sigma_n=50$ respectively, to generate the noisy image y . Fig. 4 shows the fitting results of empirical distributions of the rank residual γ on these two images. It can be observed that both empirical distributions can be reasonably well approximated by a Laplacian distribution, which is usually modeled by an ℓ_1 -norm. Therefore, Eq. (4) can now be written as

$$\hat{X}_i = \arg \min_{X_i} \left(\frac{1}{2} \|Y_i - X_i\|_F^2 + \lambda \|\gamma_i\|_1 \right). \quad (5)$$

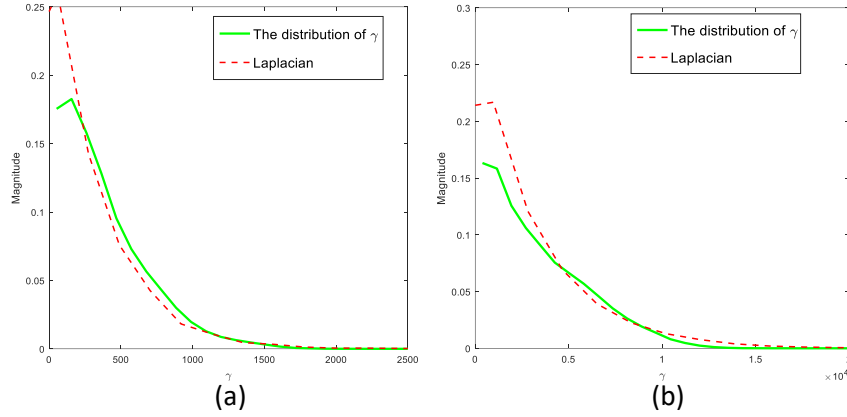


Figure 4: The distributions of the rank residual γ for image *Fence* with $\sigma_n=20$ (a) and image *Parrot* with $\sigma_n=50$ (b).

4.2 Estimate X'

In Eq. (4), after determining S_p , we also need to estimate X'_i , as the original image is not available in real applications. A variety of algorithms exist to estimate X'_i . For example, if we have many example images that are similar to the original image x , we could search for similar patches to construct the matrix X'_i from the example image set [31, 32]. However, under many practical situations, the example image set is simply unavailable. In this paper, inspired by the fact that natural images often contain repetitive structures [33], we search for nonlocal similar patches to the given patch directly in the noisy image and use the method similar to nonlocal means [24] to obtain the reference matrix $X'_i = \{x'_{i,j}\}_{j=1}^m$ by

$$x'_{i,j} = \sum_{k=1}^{m-j+1} w_{i,k} y_{i,k}, \quad (6)$$

where m is the total number of similar patches and $w_{i,k}$ is the weight, which is inversely proportional to the distance between patches y_i and $y_{i,k}$, i.e., $w_{i,k} = \frac{1}{W} \exp(-\|y_i - y_{i,k}\|_2^2/h)$, where h is a predefined constant and W is a normalization factor. It is worth noting that Eq. (6) is a recursive like algorithm based on nonlocal means.

4.3 Iterative Shrinkage Algorithm to Solve the Proposed RRC Model

We now develop an efficient algorithm to solve Eq. (5). In order to do so, we first introduce the following lemma and theorem.

Lemma 1 [34] *The minimization problem*

$$\hat{\mathbf{x}} = \arg \min_{\mathbf{x}} \left(\frac{1}{2} \|\mathbf{a} - \mathbf{x}\|_2^2 + \tau \|\mathbf{x} - \mathbf{b}\|_1 \right) \quad (7)$$

has a closed-form solution

$$\hat{\mathbf{x}} = \text{soft}(\mathbf{a} - \mathbf{b}, \tau) + \mathbf{b}, \quad (8)$$

where $\text{soft}(\mathbf{a}, \tau) = \text{sgn}(\mathbf{a}) \odot \max(\text{abs}(\mathbf{a}) - \tau, 0)$; \odot denotes the element-wise (Hadamard) product, and $\mathbf{a}, \mathbf{b}, \mathbf{x}$ are vectors of the same dimension.

Theorem 1 [35] (von Neumann) *For any two matrices $\mathbf{A}, \mathbf{B} \in \mathbb{R}^{m \times n}$, $\text{Tr}(\mathbf{A}^T \mathbf{B}) \leq \text{Tr}(\sigma(\mathbf{A})^T \sigma(\mathbf{B}))$, where Tr calculates the trace of the ensured matrix; $\sigma(\mathbf{A})$ and $\sigma(\mathbf{B})$ are the ordered singular value matrices of \mathbf{A} and \mathbf{B} with the same order, respectively.*

We now provide the solution of Eq. (5) by the following theorem.

Theorem 2 *Let $\mathbf{Y}_i = \mathbf{U}_i \Delta_i \mathbf{V}_i^T$ be the SVD (singular value decomposition) of $\mathbf{Y}_i \in \mathbb{R}^{d \times m}$ with $\Delta_i = \text{diag}(\delta_{i,1}, \dots, \delta_{i,j})$, $j = \min(d, m)$, $\mathbf{X}_i' = \mathbf{R}_i \Lambda_i \mathbf{Q}_i^T$ be the SVD of $\mathbf{X}_i' \in \mathbb{R}^{d \times m}$ with $\Lambda_i = \text{diag}(\psi_{i,1}, \dots, \psi_{i,j})$. The optimal solution \mathbf{X}_i to the problem in Eq. (5) is $\mathbf{U}_i \Sigma_i \mathbf{V}_i^T$, where $\Sigma_i = \text{diag}(\sigma_{i,1}, \dots, \sigma_{i,j})$, and the k^{th} diagonal element $\sigma_{i,k}$ is solved by*

$$\min_{\sigma_{i,k} \geq 0} \left(\frac{1}{2} (\delta_{i,k} - \sigma_{i,k})^2 + \lambda |\sigma_{i,k} - \psi_{i,k}| \right), \quad \forall k = 1, \dots, j. \quad (9)$$

Proof 1 *Supposing that the SVD of $\mathbf{X}_i, \mathbf{Y}_i, \mathbf{X}_i'$ are $\mathbf{X}_i = \mathbf{U}_i \Sigma_i \mathbf{V}_i^T$, $\mathbf{Y}_i = \mathbf{P}_i \Delta_i \mathbf{S}_i^T$ and $\mathbf{X}_i' = \mathbf{R}_i \Lambda_i \mathbf{Q}_i^T$, respectively, where Σ_i, Δ_i and Λ_i are ordered singular value matrices with the same order. Recalling Eq. (5) and from Theorem 1, we have,*

$$\begin{aligned} \|\mathbf{Y}_i - \mathbf{X}_i\|_F^2 &= \|\mathbf{P}_i \Delta_i \mathbf{S}_i^T - \mathbf{U}_i \Sigma_i \mathbf{V}_i^T\|_F^2 = \text{Tr}(\Delta_i \Delta_i^T) + \text{Tr}(\Sigma_i \Sigma_i^T) - 2\text{Tr}(\mathbf{X}_i^T \mathbf{Y}_i) \\ &\geq \text{Tr}(\Delta_i \Delta_i^T) + \text{Tr}(\Sigma_i \Sigma_i^T) - 2\text{Tr}(\Sigma_i^T \Delta_i) = \|\Delta_i - \Sigma_i\|_F^2, \end{aligned} \quad (10)$$

where the equality holds only when $\mathbf{P}_i = \mathbf{U}_i$ and $\mathbf{S}_i = \mathbf{V}_i$. Therefore, Eq. (5) is minimized when $\mathbf{P}_i = \mathbf{U}_i$ and $\mathbf{S}_i = \mathbf{V}_i$, and the optimal solution of Σ_i is obtained by solving

$$\min_{\Sigma_i \geq 0} \frac{1}{2} \|\Delta_i - \Sigma_i\|_F^2 + \lambda \sum_{k=1}^j |\gamma_{i,k}| = \min_{\sigma_{i,k} \geq 0} \sum_{k=1}^j \left(\frac{1}{2} (\delta_{i,k} - \sigma_{i,k})^2 + \lambda |\sigma_{i,k} - \psi_{i,k}| \right), \quad (11)$$

where $\sigma_{i,k}, \delta_{i,k}$ and $\psi_{i,k}$ are the k^{th} singular value of $\mathbf{X}_i, \mathbf{Y}_i$ and \mathbf{X}_i' , respectively.

Thereby, the minimization problem in Eq. (5) can be simplified by minimizing the problem in Eq. (11). For fixed $\delta_{i,k}, \psi_{i,k}$ and λ , based on Lemma 1, the closed-form solution of Eq. (11) is

$$\sigma_{i,k} = \text{soft}(\delta_{i,k} - \psi_{i,k}, \lambda) + \psi_{i,k}. \quad (12)$$

Provided the solution of Σ_i in Eq. (12), the group matrix \mathbf{X}_i can be reconstructed by $\hat{\mathbf{X}}_i = \mathbf{U}_i \Sigma_i \mathbf{V}_i$. Then the denoised image $\hat{\mathbf{x}}$ can be reconstructed by aggregating all the group matrices $\{\hat{\mathbf{X}}_i\}_{i=1}^n$.

In practical applications, we would perform the above denoising procedure several iterations to achieve better results. In the t^{th} iteration, the iterative regularization strategy [36] is used to update \mathbf{y} by

$$\mathbf{y}^t = \hat{\mathbf{x}}^{t-1} + \mu(\mathbf{y} - \mathbf{y}^{t-1}) \quad (13)$$

where μ representing the step-size. The standard deviation of the noise in the t^{th} iteration is adjusted by $\sigma_n^t = \rho \sqrt{(\sigma_n^2 - \|\mathbf{y} - \hat{\mathbf{x}}^{t-1}\|_2^2)}$, where ρ is a constant. The parameter λ that balances the fidelity term and the regularization term should also be adaptively determined in each iteration, and inspired by [37], λ of each group matrix \mathbf{Y}_i is set to

$$\lambda = \frac{c \, 2\sqrt{2} \, \sigma_n^2}{\varphi_i + \epsilon}, \quad (14)$$

where φ_i denotes the estimated variance of γ_i , and c, ϵ are small constants.

Algorithm 1 RRC for Image Denoising.

Require: Noisy image \mathbf{y} .

- 1: Initialize $\hat{\mathbf{x}}^0 = \mathbf{y}, \mathbf{y}^0 = \mathbf{y}, \sigma_n, c, d, m, L, h, \rho, \mu$ and ϵ .
 - 2: **for** $t = 1$ **to** Max-Iter **do**
 - 3: Iterative Regularization $\mathbf{y}^t = \hat{\mathbf{x}}^{t-1} + \mu(\mathbf{y} - \mathbf{y}^{t-1})$.
 - 4: **for** Each patch \mathbf{y}_i in \mathbf{y}^t **do**
 - 5: Find similar patches to construct matrix \mathbf{Y}_i .
 - 6: Perform $[\mathbf{U}_i, \mathbf{\Delta}_i, \mathbf{V}_i] = \text{SVD}(\mathbf{Y}_i)$.
 - 7: Estimate the reference matrix \mathbf{X}'_i by Eq. (6).
 - 8: Perform $[\mathbf{R}_i, \mathbf{\Lambda}_i, \mathbf{Q}_i] = \text{SVD}(\mathbf{X}'_i)$.
 - 9: Update λ by Eq. (14).
 - 10: Estimate $\mathbf{\Sigma}_i$ by Eq. (12).
 - 11: Get the estimation: $\hat{\mathbf{X}}_i = \mathbf{U}_i \mathbf{\Sigma}_i \mathbf{V}_i^T$.
 - 12: **end for**
 - 13: Aggregate \mathbf{X}_i to form the denoised image $\hat{\mathbf{x}}^t$.
 - 14: **end for**
 - 15: **Output:** The final denoised image $\hat{\mathbf{x}}$.
-

The complete description of the proposed RRC based image denoising approach to solve the problem in Eq. (5) is exhibited in Algorithm 1, corresponding to the flowchart shown in Fig. 1. Till now, we have built the model of RRC and have derived the solution of it. The next question is the feasibility of the RRC model, and we provide a theoretical analysis from the perspective of group sparse representation [25, 29, 26, 28, 30].

5 Analyzing the RRC model Using Group Sparse Representation

In this section, we provide a mathematical explanation of the proposed RRC model from the perspective of the group-based sparse representation (GSR) [25, 29, 26, 28, 30]. To this end, an adaptive dictionary for each group is introduced. Based on this designed dictionary, we bridge the gap between the proposed RRC model and GSR model. More specifically, we prove that the proposed RRC model is equivalent to a GSR model, i.e., group sparsity residual constraint (GSRC) model.

5.1 Group-based Sparse Representation

We first give a brief introduction to the GSR model. We extract n group matrices from a clean image \mathbf{x} . Similar to patch-based sparse representation, e.g., K-SVD [50], given a dictionary \mathbf{D}_i , each group $\mathbf{X}_i^* \in \mathbb{R}^{d \times m}$ can be sparsely represented by solving

$$\hat{\mathbf{B}}_i^* = \arg \min_{\mathbf{B}_i^*} \left(\frac{1}{2} \|\mathbf{X}_i - \mathbf{D}_i \mathbf{B}_i^*\|_F^2 + \lambda \|\mathbf{B}_i^*\|_1 \right), \quad (15)$$

where \mathbf{B}_i^* is the group sparse coefficient for each group \mathbf{X}_i^* and the ℓ_1 -norm is imposed on each column of \mathbf{B}_i^* , which also holds true for the following derivation with ℓ_1 -norm on matrix.

In image denoising, the goal is to use the GSR model to recover the group matrix \mathbf{X}_i^* from the *noisy* observation \mathbf{Y}_i by solving

$$\hat{\mathbf{A}}_i = \arg \min_{\mathbf{A}_i} \left(\frac{1}{2} \|\mathbf{Y}_i - \mathbf{D}_i \mathbf{A}_i\|_F^2 + \lambda \|\mathbf{A}_i\|_1 \right). \quad (16)$$

Once \mathbf{A}_i is obtained, the clean image can be reconstructed.

However, under the noisy environment, it is challenging to estimate the true group sparse coefficients \mathbf{B}_i^* from \mathbf{Y}_i directly. In other words, the group sparse coefficient \mathbf{A}_i obtained from Eq. (16) is expected to be close to the true group sparse coefficient \mathbf{B}_i^* in Eq. (15). Therefore, the quality of

image denoising largely depends on the *group sparsity residual*, which is defined by the difference between \mathbf{A}_i and \mathbf{B}_i^* ,

$$\mathbf{R}_i^* = \mathbf{A}_i - \mathbf{B}_i^*. \quad (17)$$

Similar to the RRC model, in real applications, \mathbf{X}_i^* is not available and we thus employ an estimate of it, denoted by \mathbf{X}_i' . Given \mathbf{X}_i' and the dictionary \mathbf{D}_i , the group sparse coefficient \mathbf{B}_i for each group \mathbf{X}_i' is solved by

$$\hat{\mathbf{B}}_i = \arg \min_{\mathbf{B}_i} \left(\frac{1}{2} \|\mathbf{X}_i' - \mathbf{D}_i \mathbf{B}_i\|_F^2 + \lambda \|\mathbf{B}_i\|_1 \right). \quad (18)$$

Following this, in order to reduce the group sparsity residual $\mathbf{R}_i = \mathbf{A}_i - \mathbf{B}_i$, we define the *group sparse residual constraint* (GSRC) model below,

$$\hat{\mathbf{A}}_i = \arg \min_{\mathbf{A}_i} \left(\frac{1}{2} \|\mathbf{Y}_i - \mathbf{D}_i \mathbf{A}_i\|_F^2 + \lambda \|\mathbf{A}_i - \mathbf{B}_i\|_1 \right). \quad (19)$$

We will prove that this GSRC model equals to the proposed RRC model under the following adaptive dictionary.

5.2 Adaptive Dictionary Learning

Hereby, an adaptive dictionary learning method is designed, that is, for each group $\mathbf{X}_i \in \mathbb{R}^{d \times m}$, its adaptive dictionary can be learned from its noisy observation $\mathbf{Y}_i \in \mathbb{R}^{d \times m}$.

Specifically, we apply the SVD to \mathbf{Y}_i ,

$$\mathbf{Y}_i = \mathbf{U}_i \mathbf{\Delta}_i \mathbf{V}_i^T = \sum_{k=1}^j \delta_{i,k} \mathbf{u}_{i,k} \mathbf{v}_{i,k}^T, \quad (20)$$

where $\delta_i = [\delta_{i,1}, \dots, \delta_{i,j}]$, $j = \min(d, m)$, $\mathbf{\Delta}_i = \text{diag}(\delta_i)$ is a diagonal matrix whose non-zero elements are represented by δ_i ; $\mathbf{u}_{i,k}$, $\mathbf{v}_{i,k}$ are the columns of \mathbf{U}_i and \mathbf{V}_i , respectively.

We define each dictionary atom $\mathbf{d}_{i,k}$ of the adaptive dictionary \mathbf{D}_i for each group \mathbf{Y}_i by

$$\mathbf{d}_{i,k} = \mathbf{u}_{i,k} \mathbf{v}_{i,k}^T, \quad \forall k = 1, \dots, j. \quad (21)$$

Till now, an adaptive dictionary $\mathbf{D}_i = [\mathbf{d}_{i,1}, \mathbf{d}_{i,2}, \dots, \mathbf{d}_{i,j}]$ has been learned for each group \mathbf{Y}_i .

5.3 Prove the Equivalence of RRC and GSRC

Now, let us recall the classical ℓ_1 -norm GSR problem in Eq. (15) and the adaptive dictionary defined in Eq. (21). In order to prove that RRC is equivalent to GSRC, we first introduce the following Lemma.

Lemma 2 Let $\mathbf{Y}_i = \mathbf{D}_i \mathbf{K}_i$, $\mathbf{X}_i = \mathbf{D}_i \mathbf{A}_i$, and \mathbf{D}_i is constructed by Eq. (21). We have

$$\|\mathbf{Y}_i - \mathbf{X}_i\|_F^2 = \|\mathbf{K}_i - \mathbf{A}_i\|_F^2. \quad (22)$$

Proof 2 From \mathbf{D}_i in Eq. (21) and the unitary property of \mathbf{U}_i and \mathbf{V}_i ,

$$\begin{aligned} \|\mathbf{Y}_i - \mathbf{X}_i\|_F^2 &= \|\mathbf{D}_i (\mathbf{K}_i - \mathbf{A}_i)\|_F^2 = \|\mathbf{U}_i \text{diag}(\mathbf{K}_i - \mathbf{A}_i) \mathbf{V}_i\|_F^2 \\ &= \text{Tr}(\mathbf{U}_i \text{diag}(\mathbf{K}_i - \mathbf{A}_i) \mathbf{V}_i \mathbf{V}_i^T \text{diag}(\mathbf{K}_i - \mathbf{A}_i) \mathbf{U}_i^T) \\ &= \text{Tr}(\mathbf{U}_i \text{diag}(\mathbf{K}_i - \mathbf{A}_i) \text{diag}(\mathbf{K}_i - \mathbf{A}_i) \mathbf{U}_i^T) \\ &= \text{Tr}(\text{diag}(\mathbf{K}_i - \mathbf{A}_i) \mathbf{U}_i \mathbf{U}_i^T \text{diag}(\mathbf{K}_i - \mathbf{A}_i)) \\ &= \text{Tr}(\text{diag}(\mathbf{K}_i - \mathbf{A}_i) \text{diag}(\mathbf{K}_i - \mathbf{A}_i)) \\ &= \|\mathbf{K}_i - \mathbf{A}_i\|_F^2. \end{aligned} \quad (23)$$

Based on Lemma 1 and Theorem 2, we have the following theorem.

Theorem 3 The equivalence of the RRC model in Eq. (5) and the GSRC model in Eq. (19) is satisfied under the adaptive dictionary \mathbf{D}_i in Eq. (21).

Proof 3 On the basis of Lemma 2, we have

$$\begin{aligned}\hat{\mathbf{A}}_i &= \arg \min_{\mathbf{A}_i} \left(\frac{1}{2} \|\mathbf{Y}_i - \mathbf{D}_i \mathbf{A}_i\|_F^2 + \lambda \|\mathbf{A}_i - \mathbf{B}_i\|_1 \right) \\ &= \arg \min_{\mathbf{A}_i} \left(\frac{1}{2} \|\mathbf{K}_i - \mathbf{A}_i\|_F^2 + \lambda \|\mathbf{A}_i - \mathbf{B}_i\|_1 \right) \\ &= \arg \min_{\boldsymbol{\alpha}_i} \left(\frac{1}{2} \|\boldsymbol{\kappa}_i - \boldsymbol{\alpha}_i\|_2^2 + \lambda \|\boldsymbol{\alpha}_i - \boldsymbol{\beta}_i\|_1 \right),\end{aligned}\quad (24)$$

where $\mathbf{X}_i = \mathbf{D}_i \mathbf{A}_i$ and $\mathbf{Y}_i = \mathbf{D}_i \mathbf{K}_i$. $\boldsymbol{\alpha}_i$, $\boldsymbol{\beta}_i$ and $\boldsymbol{\kappa}_i$ denote the vectorization of the matrix \mathbf{A}_i , \mathbf{B}_i and \mathbf{K}_i , respectively.

Following this, based on Lemma 1, we have

$$\boldsymbol{\alpha}_i = \text{soft}(\boldsymbol{\kappa}_i - \boldsymbol{\beta}_i, \lambda) + \boldsymbol{\beta}_i. \quad (25)$$

Obviously, according to Eqs. (20) and (21),

$$\begin{aligned}\mathbf{D}_i \hat{\mathbf{A}}_i &= \sum_{k=1}^j \left(\text{soft}(\boldsymbol{\kappa}_{i,k} - \boldsymbol{\beta}_{i,k}, \lambda) + \boldsymbol{\beta}_{i,k} \right) \mathbf{d}_{i,k} \\ &= \sum_{k=1}^j \left(\text{soft}(\boldsymbol{\kappa}_{i,k} - \boldsymbol{\beta}_{i,k}, \lambda) + \boldsymbol{\beta}_{i,k} \right) \mathbf{u}_{i,k} \mathbf{v}_{i,k}^T \\ &= \mathbf{U}_i \hat{\mathbf{A}}_i \mathbf{V}_i^T = \hat{\mathbf{X}}_i,\end{aligned}\quad (26)$$

where $\boldsymbol{\kappa}_{i,k}$, $\boldsymbol{\beta}_{i,k}$ represent the k^{th} element in the i^{th} group sparse coefficient $\boldsymbol{\kappa}_i$ and $\boldsymbol{\beta}_i$, respectively.

Therefore, based on the adaptive dictionary \mathbf{D}_i in Eq. (21) and Theorem 1, we have proved that Eq. (25) is equivalent to Eq. (12). We thus have that RRC is equivalent to GSRC, i.e.,

$$\begin{aligned}\hat{\mathbf{X}}_i &= \arg \min_{\mathbf{X}_i} \left(\frac{1}{2} \|\mathbf{Y}_i - \mathbf{X}_i\|_F^2 + \lambda \|\boldsymbol{\gamma}_i\|_1 \right) \\ &\quad \updownarrow \\ \hat{\mathbf{A}}_i &= \arg \min_{\mathbf{A}_i} \left(\frac{1}{2} \|\mathbf{Y}_i - \mathbf{D}_i \mathbf{A}_i\|_F^2 + \lambda \|\mathbf{A}_i - \mathbf{B}_i\|_1 \right).\end{aligned}\quad (27)$$

Obviously, according to the above analysis, we bridge the gap between the proposed RRC model and GSR model. It is worth noting that the dictionary can be learned in various manners and the proposed adaptive dictionary learning approach is just one example. There are extensive researches on the sparsity residual model for image processing and we have witnessed great successes of these models [39, 51–53]. Although the designed adaptive dictionary learning seems to translate the sparse representation into the rank minimization problem, the main difference between sparse representation and the rank minimization models is that sparse representation has a dictionary learning process while the rank minimization problem does not, to the best of our knowledge. This is also the key difference between our RRC model and the NCSR method [39]. Therefore, encouraged by this and since we have proved the equivalence between the proposed RRC model and the GSRC model based on the designed dictionary, we are confident on the feasibility of the RRC model for image processing, which will be further validated by extensive experiments on image denoising in the following section.



Figure 5: The 12 test images: Lena, Leaves, Monarch, Airplane, House, Parrot, Starfish, Fence, Foreman, J.Bean, Barbara, Plants.

6 Experimental Results

In this section, we conduct experiments to validate the performance of the proposed RRC model and compare it with leading denoising methods, including BM3D [25], EPLL [27], Plow [38], NCSR [39], PID [40], PGPD [28], LINC [41], aGMM [42] and NNM. Except NNM, the source codes of all the competing methods are obtained from the original authors and we used the default parameter settings. The parameter settings of the proposed RRC model are as follows. The size of each patch $\sqrt{d} \times \sqrt{d}$ is set to 6×6 , 7×7 , 8×8 and 9×9 for $\sigma_n \leq 20$, $20 < \sigma_n \leq 50$, $50 < \sigma_n \leq 75$ and $75 < \sigma_n \leq 100$, respectively. The searching window for similar patches is set to $L = 25$; $\epsilon = 0.2$, $h = 40$. The parameters (μ, ρ, c, m, τ) are set to $(0.1, 0.9, 0.9, 60, 0.001)$, $(0.1, 0.8, 0.9, 60, 0.001)$, $(0.1, 0.8, 0.9, 70, 0.0006)$, $(0.1, 0.8, 1, 80, 0.0006)$, $(0.1, 0.8, 1, 90, 0.0005)$ and $(0.1, 0.8, 1, 100, 0.002)$ for $\sigma_n \leq 20$, $20 < \sigma_n \leq 30$, $30 < \sigma_n \leq 40$, $40 < \sigma_n \leq 50$, $50 < \sigma_n \leq 75$ and $75 < \sigma_n \leq 100$, respectively. We set the stopping criterion to $\|\hat{\mathbf{x}}^t - \hat{\mathbf{x}}^{t-1}\|_2 / \|\hat{\mathbf{x}}^{t-1}\|_2 < \tau$, where τ is a small constant. The source code of the proposed RRC for image denoising can be downloaded at: https://drive.google.com/open?id=1XfW6_lsv0p7LzU7Wjzve9YNLuG3uZvei.

We evaluate the competing methods on 12 widely used test images shown in Fig. 5, namely *Lena*, *Leaves*, *Monarch*, *Airplane*, *House*, *Parrot*, *Starfish*, *Fence*, *Foreman*, *J.Bean*, *Barbara* and *Plants*. Here, we present the denoising results at four noise levels, i.e., $\sigma_n = \{30, 50, 75, 100\}$. The PSNR and SSIM results under these noise levels for all methods are shown in Table 1. It can be seen that the proposed RRC algorithm outperforms other competing methods in most cases in terms of PSNR. The average gains of the proposed RRC over BM3D, EPLL, Plow, NCSR, PID, PGPD, LINC, aGMM and NNM methods are as much as 0.25dB, 0.84dB, 0.82dB, 0.45dB, 0.18dB, 0.18dB, 0.37dB, 0.62dB and 1.54dB, respectively. It is clear that the proposed RRC significantly outperforms the representative rank minimization method, namely, NNM. One can also observe that the proposed RRC achieves higher SSIM results than other competing methods. In particular, under high noise level $\sigma_n = 100$, the proposed RRC consistently outperforms other competing methods for all test images. The only exception is the image *J.Bean* for which NCSR is slightly (0.0029) better on SSIM [49]. The visual comparisons of different denoising methods are shown in Figs. 6-7. Obviously, NNM generates the worst perceptual result. One can observe that EPLL, Plow, NCSR, PGPD and aGMM still suffer from some undesirable artifacts, while BM3D, PID and LINC tend to over-smooth the image. By contrast, the proposed RRC not only removes most of the visual artifacts, but also preserves large scale sharp edges and small-scale image details.

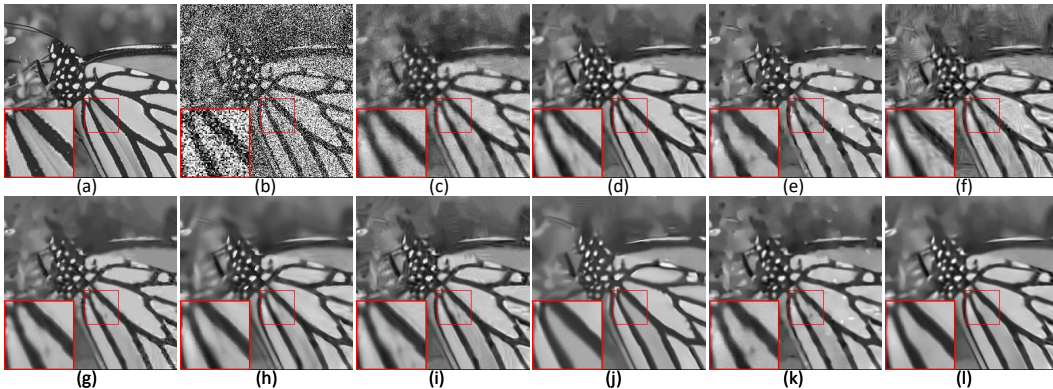


Figure 6: Denoising results of *Monarch* with $\sigma_n = 100$. (a) Original image; (b) Noisy image; (c) NNM (PSNR=21.03dB); (d) BM3D (PSNR=22.52dB); (e) EPLL (PSNR =22.24dB); (f) Plow (PSNR = 21.83dB); (g) NCSR (PSNR = 22.10dB); (h) PID (PSNR =22.59dB); (i) PGPD (PSNR =22.56dB); (j) LINC (PSNR =22.13dB); (k) aGMM (PSNR =22.42dB); (l) RRC (PSNR =**22.76dB**).

We also compare the proposed RRC with WNNM [16] method, which is a well-known rank minimization method that delivers state-of-the-art denoising results. The PSNR/SSIM results are shown in the last two columns of Table 1. It can be seen that though the PSNR results of RRC is slightly (< 0.2 dB) lower than WNNM, the SSIM results of the proposed RRC is higher (~ 0.01) than WNNM when the noise level $\sigma_n \geq 50$. It is well-known that SSIM is consistent with the human visual system and leads to more accurate results. The visual comparison of RRC and WNNM with one exemplar image is shown in Fig. 8, where we can observe that more details are recovered by RRC than WNNM. Our proposed RRC model is an optimization based algorithm. The running time of RRC is faster than

Table 1: PSNR in dB (top entry in each cell) and SSIM (bottom entry) results of different denoising methods.

Images	$\sigma_n = 30$										$\sigma_n = 50$											
	NNM	BM3D	EPLL	Plow	NCSR	PID	PGPD	LINC	aGMM	WNNM	RRC	NNM	BM3D	EPLL	Plow	NCSR	PID	PGPD	LINC	aGMM	WNNM	RRC
Airplane	27.62 0.7441	28.49 0.8631	28.54 0.8628	28.03 0.8532	28.34 0.8660	28.69 0.8734	28.63 0.8646	28.53 0.8632	28.42 0.8647	28.82 0.8717	28.63 0.8716	25.16 0.6839	25.76 0.8044	25.96 0.7922	25.64 0.8066	25.63 0.8066	26.09 0.8163	25.98 0.8059	26.04 0.8021	25.83 0.7990	26.32 0.8121	26.13 0.8172
Barbara	28.08 0.7924	29.08 0.8618	27.58 0.8209	28.99 0.8597	28.68 0.8524	29.07 0.8670	28.93 0.8565	29.53 0.8780	27.88 0.8129	29.67 0.8790	29.51 0.8736	25.66 0.7004	26.42 0.7698	24.86 0.6943	26.42 0.7663	26.13 0.7572	26.58 0.7802	26.27 0.7613	26.27 0.7612	25.37 0.7021	26.83 0.7925	26.78 0.7872
Fence	27.43 0.7785	28.19 0.8326	27.22 0.8150	27.59 0.8182	28.13 0.8298	28.20 0.8318	28.23 0.8255	27.31 0.8286	27.31 0.8021	28.61 0.8382	28.25 0.8246	25.92 0.6988	25.92 0.7621	25.92 0.7162	26.90 0.7496	25.49 0.7476	25.77 0.7557	25.94 0.7573	25.94 0.7535	25.94 0.7010	25.94 0.7777	25.97 0.7561
Foreman	30.24 0.7216	32.75 0.8823	31.70 0.8617	32.45 0.8698	32.61 0.8846	33.09 0.8923	32.83 0.8818	32.93 0.8894	32.31 0.8766	32.99 0.8952	32.38 0.6983	28.69 0.8445	30.36 0.8051	29.20 0.7976	29.60 0.8559	29.60 0.8585	30.41 0.8410	30.63 0.8534	29.80 0.8270	29.80 0.8508	30.75 0.8611	30.87 0.8508
House	29.85 0.7118	32.09 0.8480	31.24 0.8383	31.67 0.8479	32.01 0.8503	32.10 0.8471	32.24 0.8485	32.26 0.8435	31.79 0.8495	32.58 0.8527	32.30 0.6780	28.00 0.8122	29.69 0.7845	28.79 0.7699	28.99 0.8160	29.61 0.8140	29.58 0.8125	29.97 0.8180	29.87 0.8002	29.28 0.8226	30.23 0.8247	29.92 0.8247
J.Bean	29.77 0.7572	31.97 0.9357	31.55 0.9240	31.61 0.9204	31.99 0.9435	31.99 0.9462	31.96 0.9317	31.99 0.9449	31.82 0.9413	32.50 0.9408	32.38 0.7293	27.77 0.9006	29.26 0.8677	28.73 0.8430	28.66 0.8430	29.24 0.9134	29.29 0.9131	29.09 0.8934	29.09 0.9085	29.01 0.8911	29.46 0.9046	29.38 0.9125
Leaves	27.17 0.8780	27.81 0.9278	27.19 0.9197	27.00 0.9057	28.04 0.9311	27.87 0.9315	27.99 0.9300	27.99 0.9339	27.53 0.9273	28.61 0.9414	28.35 0.9366	24.22 0.8250	24.68 0.8680	24.39 0.8638	24.28 0.8354	24.94 0.8787	25.01 0.8817	25.03 0.8794	25.11 0.8925	24.42 0.8673	25.58 0.9015	25.30 0.8910
Lena	0.7543 0.7543	0.8584 0.8477	0.8477 0.8493	0.8580 0.8580	0.8650 0.8650	0.8622 0.8668	0.8548 0.8548	0.8595 0.8595	0.8672 0.8696	0.7920 0.7732	0.7691 0.8009	25.30 0.7988	25.82 0.7990	25.78 0.7976	25.41 0.7988	26.21 0.7988	25.73 0.7990	25.88 0.7976	25.82 0.7820	25.82 0.8020	26.27 0.8073	26.22 0.8073
Monarch	27.63 0.7980	28.36 0.8822	28.36 0.8789	27.77 0.8714	28.38 0.8829	28.63 0.8909	28.49 0.8853	28.74 0.8970	28.27 0.8831	29.13 0.8999	28.79 0.8954	25.30 0.7428	25.82 0.8200	25.78 0.8124	25.41 0.7910	26.21 0.8252	25.73 0.8338	25.88 0.8269	25.82 0.8314	25.82 0.8164	26.27 0.8369	26.22 0.8361
Parrot	0.7337 0.7337	0.8705 0.8569	0.8617 0.8617	0.8705 0.8780	0.8681 0.8681	0.8744 0.8744	0.8671 0.8671	0.8740 0.8740	0.8671 0.8671	0.8780 0.8780	0.8654 0.8654	26.77 0.7669	27.88 0.7479	27.28 0.7327	27.26 0.7589	27.67 0.7589	28.26 0.7669	27.91 0.7669	28.23 0.7636	28.23 0.7561	28.23 0.7745	28.32 0.7789
Plants	29.09 0.7141	30.70 0.8373	30.43 0.8278	30.41 0.8270	30.19 0.8273	30.86 0.8395	30.73 0.8370	30.67 0.8393	30.50 0.8314	30.94 0.8459	30.90 0.6545	27.05 0.7669	28.11 0.7479	27.83 0.7327	27.75 0.7589	27.65 0.7589	28.31 0.7669	28.25 0.7669	27.96 0.7636	28.00 0.7561	28.25 0.7745	28.32 0.7789
Starfish	27.24 0.7725	27.65 0.8289	27.52 0.8248	27.02 0.8075	27.69 0.8283	27.69 0.8180	27.67 0.8277	27.52 0.8195	27.61 0.8263	28.50 0.8378	27.95 0.8304	24.58 0.6887	25.04 0.7433	25.05 0.7392	24.71 0.7175	25.06 0.7440	24.80 0.7293	25.11 0.7457	24.81 0.7326	25.09 0.7419	25.34 0.7529	25.34 0.7589
Average	28.47 0.7630	29.24 0.8690	29.21 0.8562	29.30 0.8569	29.63 0.8685	29.63 0.8737	29.63 0.8681	29.79 0.8736	29.48 0.8609	29.78 0.8765	30.04 0.7076	27.15 0.8093	26.61 0.7830	26.74 0.7774	27.06 0.8113	27.31 0.8155	27.27 0.8095	27.27 0.8127	26.86 0.7918	27.27 0.8223	27.27 0.8223	
Images	$\sigma_n = 75$										$\sigma_n = 100$											
	NNM	BM3D	EPLL	Plow	NCSR	PID	PGPD	LINC	aGMM	WNNM	RRC	NNM	BM3D	EPLL	Plow	NCSR	PID	PGPD	LINC	aGMM	WNNM	RRC
Airplane	23.15 0.5493	23.99 0.7488	24.03 0.7168	23.67 0.6589	23.76 0.7547	24.08 0.7536	24.15 0.7475	23.81 0.7248	23.95 0.7248	24.20 0.7637	24.10 0.7570	21.75 0.4897	22.78 0.7036	22.30 0.6523	22.60 0.7107	22.82 0.7083	22.42 0.6941	22.42 0.6931	22.67 0.6571	22.93 0.7075	23.02 0.7209	22.93 0.7209
Barbara	23.58 0.5691	24.53 0.6798	23.08 0.5848	24.30 0.6548	24.06 0.6616	24.67 0.6879	24.03 0.6613	23.09 0.5882	23.09 0.5882	24.79 0.6964	24.62 0.6825	22.01 0.5026	23.20 0.6092	21.89 0.5135	22.86 0.5647	22.70 0.5960	23.37 0.6179	23.11 0.6039	21.92 0.5773	23.27 0.5163	23.27 0.6243	23.27 0.6243
Fence	23.22 0.5890	24.22 0.6962	22.46 0.6076	23.57 0.6586	23.75 0.6742	24.20 0.6857	24.18 0.6872	23.81 0.6750	22.70 0.6098	24.53 0.7108	24.32 0.6924	21.62 0.5044	22.92 0.6362	21.10 0.5727	22.17 0.6009	22.23 0.6313	23.00 0.6226	22.87 0.6184	22.34 0.5386	21.50 0.6753	23.08 0.6407	
Foreman	26.18 0.5524	28.07 0.7933	27.24 0.7467	27.15 0.7067	28.18 0.8171	28.40 0.8186	28.39 0.7965	28.11 0.8162	27.67 0.7676	28.49 0.8099	28.83 0.8259	24.79 0.5160	26.51 0.7489	25.91 0.6329	25.55 0.7833	26.55 0.7888	26.96 0.7452	26.81 0.7826	26.55 0.7129	27.20 0.7817	27.27 0.7969	
House	25.56 0.5439	27.51 0.7645	26.70 0.7251	26.52 0.6733	27.16 0.7749	27.35 0.7723	27.81 0.7709	27.56 0.7850	27.11 0.7419	28.46 0.7950	27.98 0.4918	23.66 0.7203	25.87 0.6695	25.21 0.5874	24.72 0.7397	25.49 0.7349	25.75 0.7195	26.17 0.7550	26.11 0.6854	25.55 0.6854	27.04 0.7655	26.38 0.7655
J.Bean	25.23 0.5796	27.22 0.8573	26.57 0.8019	26.23 0.7422	27.15 0.8792	27.06 0.8730	27.07 0.8503	26.62 0.8669	27.09 0.8243	27.20 0.8637	27.17 0.8749	23.73 0.5341	25.80 0.8181	25.16 0.7429	24.55 0.6574	25.61 0.8472	25.55 0.8386	25.66 0.7999	24.88 0.8339	25.58 0.7628	25.64 0.8188	25.71 0.8443
Leaves	21.79 0.6408	22.49 0.7288	22.03 0.6968	22.02 0.6723	22.60 0.7415	22.61 0.7350	22.45 0.7358	21.96 0.7101	21.96 0.7101	23.13 0.7498	22.92 0.8377	19.57 0.6345	20.90 0.7482	20.26 0.7163	20.43 0.6814	20.84 0.7622	20.77 0.7405	20.95 0.7469	20.49 0.7499	20.29 0.7106	21.56 0.7946	21.22 0.7811
Lena	24.08 0.5647	25.17 0.7288	24.75 0.6968	24.64 0.6723	25.02 0.7415	25.16 0.7350	25.30 0.7358	25.12 0.7101	25.02 0.7101	25.38 0.7498	25.33 0.5093	23.30 0.6739	23.87 0.6345	23.46 0.5895	23.19 0.6906	23.63 0.6874	23.91 0.6874	24.02 0.6845	23.67 0.6487	23.73 0.6487	24.07 0.7100	24.14 0.7100
Monarch	23.06 0.6206	23.91 0.7557	23.73 0.6917	23.34 0.6255	23.67 0.7007	24.22 0.7011	24.00 0.6998	23.91 0.6805	23.85 0.6805	24.16 0.7172	21.03 0.7172	22.52 0.4789	22.24 0.6525	21.83 0.6129	22.10 0.5531	22.10 0.6587	22.10 0.6587	22.59 0.6472	22.36 0.6495	22.13 0.6210	22.42 0.7312	22.76 0.7312
Parrot	24.54 0.5567	25.94 0.7771	25.56 0.7399	25.15 0.6859	25.45 0.7892	26.28 0.7979	25.98 0.7775	26.20 0.7988	25.72 0.7555	26.33 0.8028	26.22 0.5197	22.84 0.7345	24.60 0.6844	24.08 0.6096	23.65 0.7518	23.94 0.7671	24.85 0.7251	24.52 0.7721	24.48 0.6979	24.26 0.6979	24.86 0.7729	24.83 0.7729
Plants	24.80 0.5107	26.25 0.7006	25.90 0.6720	25.57 0.6255	25.75 0.7007	26.30 0.7011	26.33 0.6998	25.90 0.6805	26.05 0.6805	26.26 0.7103	26.40 0.7172	22.27 0.4789	24.98 0.6525	24.65 0.6129	24.14 0.5531	24.46 0.6587	24.99 0.6587	25.06 0.6472	24.36 0.6495	24.75 0.6210	24.88 0.6680	24.91 0.6680
Starfish	22.52 0.5617	23.27 0.6670	23.17 0.6502	22.82 0.6192	23.18 0.6685	22.89 0.6422	23.23 0.6638	22.74 0.6416	23.22 0.6525	23.25 0.6659	23.32 0.6741	20.97 0.4979	22.10 0.6053	21.92 0.5799	21.48 0.6062	21.91 0.5760	21.63 0.6018	22.08 0.5635	21.10 0.5813	21.95 0.6176	22.05 0.6176	21.98 0.6081
Average	23.98 0.5770	25.21 0.7480	24.60 0.7061	24.58 0.6784	24.98 0.7543	25.27 0.7548	25.29 0.7520	25.02 0.7156	24.78 0.7156	25.52 0.7662	25.45 0.5199	22.21 0.6961	23.85 0.6420	23.22 0.5974	23.07 0.7049	23.50 0.7053	23.85 0.6989	23.90 0.6989	23.41 0.6512	23.40 0.7161	24.05 0.7220	

NCSR, and about twice long as NNM, and it is very close to WNNM. Such experimental findings clearly demonstrate that the proposed RRC model is a powerful prior for the class of photographic images containing large variations in edges/textures.

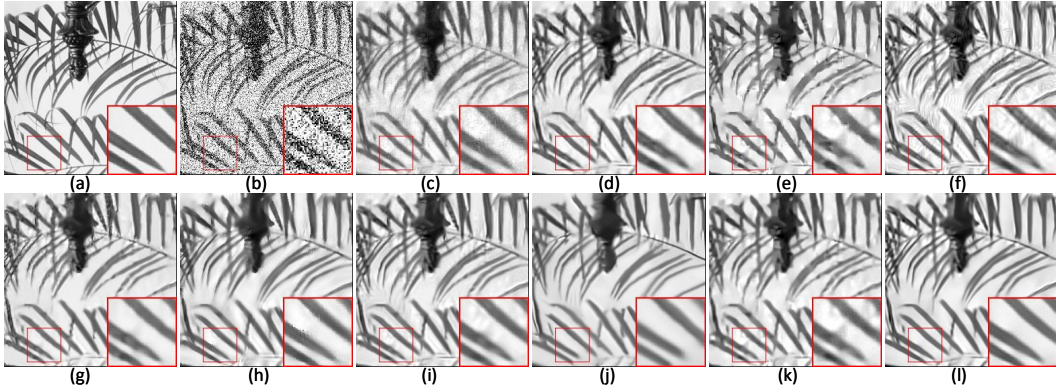


Figure 7: Denoising results of *Leaves* with $\sigma_n=100$. (a) Original image; (b) Noisy image; (c) NNM (PSNR=19.57dB); (d) BM3D (PSNR=20.90dB); (e) EPLL (PSNR =20.26dB); (f) Plow (PSNR = 20.43dB); (g) NCSR (PSNR = 20.84dB); (h) PID (PSNR =20.77dB); (i) PGPD (PSNR =20.95dB); (j) LINC (PSNR =20.49dB); (k) aGMM (PSNR =20.29dB); (l) RRC (PSNR =21.22dB).

7 Conclusion

We have proposed a new method, called rank residual constraint, to reinterpret the rank minimization problem from the perspective of matrix approximation. Via minimizing the rank residual, we have developed a high performance low-rank matrix approximation algorithm. Based on the group-based sparse representation model, a mathematical explanation on the feasibility of the RRC model has

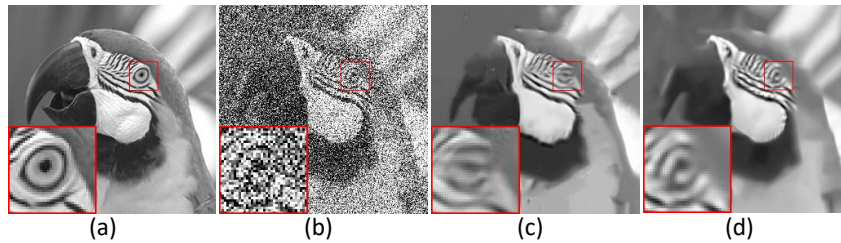


Figure 8: Denoising results of WNNM and RRC at $\sigma_n=100$. (a) Original *Parrot* image; (b) Noisy image; (c) WNNM (PSNR=**24.86dB**, SSIM = 0.7529); (d) RRC (PSNR= 24.83dB, SSIM =**0.7729**).

been derived. We have applied the proposed RRC model to image denoising by exploiting the image nonlocal self-similarity prior. Experimental results have demonstrated that our proposed RRC model not only leads to visible quantitative improvements over many state-of-the-art methods, but also preserves the image local structures and suppresses undesirable artifacts. Our RRC model is inspired by the spirit of GAN in deep learning, and we expect more ideas and underlying principles can be shared between the deep learning based networks and the optimization based methods.

References

- [1] Candès E J, Li X, Ma Y, et al. Robust principal component analysis?[J]. *Journal of the ACM (JACM)*, 2011, 58(3): 11.
- [2] Peng Y, Ganesh A, Wright J, et al. RASL: Robust alignment by sparse and low-rank decomposition for linearly correlated images[J]. *IEEE transactions on pattern analysis and machine intelligence*, 2012, 34(11): 2233-2246.
- [3] Liu G, Lin Z, Yu Y. Robust Subspace Segmentation by Low-Rank Representation[C]// *International Conference on Machine Learning*. DBLP, 2010:663-670.
- [4] Ji H, Liu C, Shen Z, et al. Robust video denoising using low rank matrix completion[C]// *Computer Vision and Pattern Recognition*. IEEE, 2010:1791-1798.
- [5] Fazel M. Matrix rank minimization with applications[D]. PhD thesis, Stanford University, 2002.
- [6] Eriksson A, Hengel A V D. Efficient computation of robust low-rank matrix approximations in the presence of missing data using the L1 norm[C]// *Computer Vision and Pattern Recognition*. IEEE, 2010:771-778.
- [7] Gu S, Zhang L, Zuo W, et al. Weighted Nuclear Norm Minimization with Application to Image Denoising[C]// *Computer Vision and Pattern Recognition*. IEEE, 2014:2862-2869.
- [8] Wright J, Ganesh A, Rao S, et al. Robust Principal Component Analysis: Exact Recovery of Corrupted Low-Rank Matrices via Convex Optimization[C]// *Neural Networks for Signal Processing X, 2000. Proceedings of the 2000 IEEE Signal Processing Society Workshop*. IEEE, 2009:289-298 vol.1.
- [9] Candès E J, Recht B. Exact Matrix Completion via Convex Optimization[J]. *Foundations of Computational Mathematics*, 2009, 9(6):717.
- [10] Salakhutdinov R, Srebro N. Collaborative Filtering in a Non-Uniform World: Learning with the Weighted Trace Norm[J]. *Advances in Neural Information Processing Systems*, 2010:2056-2064.
- [11] Zhao Q, Meng D, Xu Z, et al. L1 -norm low-rank matrix factorization by variational Bayesian method.[J]. *IEEE Transactions on Neural Networks & Learning Systems*, 2017, 26(4):825-839.
- [12] Srebro N, Jaakkola T. Weighted Low-Rank Approximations[C]// *International Conference on Machine Learning*. 2003:720-727.
- [13] Salakhutdinov R, Mnih A. Probabilistic Matrix Factorization[C]// *International Conference on Neural Information Processing Systems*. Curran Associates Inc. 2007:1257-1264.
- [14] Kong Y, Shao M, Li K, et al. Probabilistic Low-Rank Multitask Learning.[J]. *IEEE Transactions on Neural Networks & Learning Systems*, 2017, PP(99):1-11.
- [15] Cai J F, Cand, S, E J, et al. A Singular Value Thresholding Algorithm for Matrix Completion[J]. *Siam Journal on Optimization*, 2008, 20(4):1956-1982.
- [16] Gu S, Xie Q, Meng D, et al. Weighted Nuclear Norm Minimization and Its Applications to Low Level Vision[J]. *International Journal of Computer Vision*, 2017, 121(2):183-208.

- [17] Xie Y, Gu S, Liu Y, et al. Weighted Schatten, p -Norm Minimization for Image Denoising and Background Subtraction[J]. IEEE Transactions on Image Processing, 2016, 25(10):4842-4857.
- [18] Nie F, Huang H, Ding C. Low-rank matrix recovery via efficient Schatten p -norm minimization[C]// Twenty-Sixth AAAI Conference on Artificial Intelligence. AAAI Press, 2012:655-661.
- [19] Liu L, Huang W, Chen D R. Exact minimum rank approximation via Schatten p norm minimization [J]. Journal of Computational & Applied Mathematics, 2014, 267(6):218-227.
- [20] Lu C, Zhu C, Xu C, et al. Generalized Singular Value Thresholding[C]//AAAI. 2015: 1805-1811.
- [21] Hu Y, Zhang D, Ye J, et al. Fast and Accurate Matrix Completion via Truncated Nuclear Norm Regularization[J]. IEEE Transactions on Pattern Analysis and Machine Intelligence, 2013, 35(9):2117-2130.
- [22] Lu C, Tang J, Yan S, et al. Generalized Nonconvex Nonsmooth Low-Rank Minimization[J]. 2014:4130-4137.
- [23] Candes E J, Wakin M B, Boyd S P. Enhancing sparsity by reweighted ℓ_1 minimization[J]. Journal of Fourier analysis and applications, 2008, 14(5-6): 877-905.
- [24] Buades A, Coll B, Morel J M. A Non-Local Algorithm for Image Denoising[C]// Computer Vision and Pattern Recognition, 2005. CVPR 2005. IEEE Computer Society Conference on. IEEE, 2005:60-65 vol. 2.
- [25] Dabov K, Foi A, Katkovnik V, et al. Image Denoising by Sparse 3-D Transform-Domain Collaborative Filtering[J]. IEEE Transactions on Image Processing A Publication of the IEEE Signal Processing Society, 2007, 16(8):2080.
- [26] Mairal J, Bach F, Ponce J, et al. Non-local sparse models for image restoration[C]// IEEE, International Conference on Computer Vision. IEEE, 2010:2272-2279.
- [27] Zoran D, Weiss Y. From learning models of natural image patches to whole image restoration[C]//Computer Vision (ICCV), 2011 IEEE International Conference on. IEEE, 2011: 479-486.
- [28] Xu J, Zhang L, Zuo W, et al. Patch group based nonlocal self-similarity prior learning for image denoising[C]//Proceedings of the IEEE international conference on computer vision. 2015: 244-252.
- [29] Dong W, Shi G, Ma Y, et al. Image Restoration via Simultaneous Sparse Coding: Where Structured Sparsity Meets Gaussian Scale Mixture[J]. International Journal of Computer Vision, 2015, 114(2-3):217-232.
- [30] Zhang J, Zhao D, Gao W. Group-based sparse representation for image restoration[J]. IEEE Transactions on Image Processing, 2014, 23(8): 3336-3351.
- [31] Li Y, Dong W, Shi G, et al. Learning parametric distributions for image super-resolution: Where patch matching meets sparse coding[C]//Proceedings of the IEEE International Conference on Computer Vision. 2015: 450-458.
- [32] Yue H, Sun X, Yang J, et al. Image denoising by exploring external and internal correlations[J]. IEEE Transactions on Image Processing, 2015, 24(6): 1967-1982.
- [33] Buades A, Coll B, Morel J M. A review of image denoising algorithms, with a new one[J]. Multiscale Modeling & Simulation, 2005, 4(2): 490-530.
- [34] Daubechies I, Defrise M, De Mol C. An iterative thresholding algorithm for linear inverse problems with a sparsity constraint[J]. Communications on Pure and Applied Mathematics: A Journal Issued by the Courant Institute of Mathematical Sciences, 2004, 57(11): 1413-1457.
- [35] Mirsky L. A trace inequality of John von Neumann[J]. Monatshefte für mathematik, 1975, 79(4): 303-306.
- [36] Osher S, Burger M, Goldfarb D, et al. An iterative regularization method for total variation-based image restoration[J]. Multiscale Modeling & Simulation, 2005, 4(2): 460-489.
- [37] Chang S G, Yu B, Vetterli M. Adaptive wavelet thresholding for image denoising and compression[J]. IEEE transactions on image processing, 2000, 9(9): 1532-1546.
- [38] Chatterjee P, Milanfar P. Patch-based near-optimal image denoising[J]. IEEE Transactions on Image Processing, 2012, 21(4): 1635.
- [39] Dong W, Zhang L, Shi G, et al. Nonlocally centralized sparse representation for image restoration[J]. IEEE Transactions on Image Processing, 2013, 22(4): 1620-1630.

- [40] Knaus C, Zwicker M. Progressive image denoising[J]. IEEE transactions on image processing, 2014, 23(7): 3114-3125.
- [41] Niknejad M, Rabbani H, Babaie-Zadeh M. Image restoration using Gaussian mixture models with spatially constrained patch clustering[J]. IEEE Transactions on Image Processing, 2015, 24(11): 3624-3636.
- [42] Luo E, Chan S H, Nguyen T Q. Adaptive image denoising by mixture adaptation[J]. IEEE transactions on image processing, 2016, 25(10): 4489-4503.
- [43] Goodfellow I, Pouget-Abadie J, Mirza M, et al. Generative adversarial nets[C]//Advances in neural information processing systems. 2014: 2672-2680.
- [44] Goodfellow I, Bengio Y, Courville A, et al. Deep learning[M]. Cambridge: MIT press, 2016.
- [45] Isola P, Zhu J Y, Zhou T, et al. Image-to-image translation with conditional adversarial networks[J]. arXiv preprint, 2017.
- [46] Reed S, Akata Z, Yan X, et al. Generative adversarial text to image synthesis[C]// International Conference on International Conference on Machine Learning. JMLR.org, 2016:1060-1069.
- [47] Denton E L, Chintala S, Fergus R. Deep generative image models using a laplacian pyramid of adversarial networks[C]//Advances in neural information processing systems. 2015: 1486-1494.
- [48] Zha Z, Liu X, Zhou Z, et al. Image denoising via group sparsity residual constraint[C]//Acoustics, Speech and Signal Processing (ICASSP), 2017 IEEE International Conference on. IEEE, 2017: 1787-1791.
- [49] Wang Z, Bovik A C, Sheikh H R, et al. Image quality assessment: from error visibility to structural similarity[J]. IEEE transactions on image processing, 2004, 13(4): 600-612.
- [50] Aharon M, Elad M, Bruckstein A. K-SVD: An algorithm for designing overcomplete dictionaries for sparse representation[J]. IEEE Transactions on signal processing, 2006, 54(11): 4311.
- [51] Liu H, Xiong R, Zhang J, et al. Image denoising via adaptive soft-thresholding based on non-local samples[C]// Computer Vision and Pattern Recognition. IEEE, 2015:484-492.
- [52] Zhao C, Ma S, Zhang J, et al. Video compressive sensing reconstruction via reweighted residual sparsity[J]. IEEE Transactions on Circuits and Systems for Video Technology, 2017, 27(6): 1182-1195.
- [53] Zha Z, Zhang X, Wang Q, et al. Group Sparsity Residual with Non-Local Samples for Image Denoising[J]. arXiv preprint arXiv:1803.08412, 2018.